Journal of Physics B: Atomic, Molecular and Optical Physics

Simultaneous measurements of strong-field ionization and high harmonic generation in aligned molecules

To cite this article before publication: Claude Marceau *et al* 2020 *J. Phys. B: At. Mol. Opt. Phys.* in press https://doi.org/10.1088/1361-6455/ab7643

Simultaneous Measurements of Strong-Field Ionization and High Harmonic Generation in Aligned Molecules

C. Marceau[1], J. B. Bertrand[1], Peng Peng[1], H. J. Wörner[1,2], P. B. Corkum[1] and D. M. Villeneuve[1]

[1]Joint Attosecond Science Laboratory, National Research Council and University of Ottawa, 100 Sussex Drive, Ottawa, ON K1A 0R6, Canada
[2]Laboratorium für physikalische Chemie, ETH Zürich, Wolfgang-Pauli-Strasse 10, 8093 Zürich, Switzerland

(Dated: January 24, 2020)

High harmonic spectroscopy relies on high harmonic generation in aligned molecules. The first step of high harmonic generation is the ionization of the molecule in the intense femtosecond laser field. Here we present measurements of both ionization yield and high harmonic yield as a function of molecular angle in N_2 and CO_2 molecules. Measurements were done at two wavelengths, 800 nm and 1200 nm, and for a range of laser intensities, to study the sensitivity of laser conditions on both processes. The behavior of N_2 was relatively insensitive to laser conditions. However in CO_2, a minimum in high harmonic emission was observed that was sensitive to both laser intensity and wavelength, and was attributed to interference in emission from the HOMO and HOMO-2 orbitals.

I. INTRODUCTION

High harmonic generation (HHG) has proven to be a sensitive probe of electronic structure in molecules, allowing angström-size reconstruction of molecular orbitals [1–3]. It holds the promise of probing the instantaneous electronic structure of a molecule during a chemical reaction [4]. Up to date, a broad range of time-resolved experiments have confirmed the sensitivity of HHG to molecular dynamics [5] such as: rotation [6, 7], vibration [8, 9], bound [10] and chemically-induced unbound nuclear motion [11]. Another class of dynamics, electron-hole dynamics [12, 13], resulting from the participation of multiple electronic states has been inferred from high-harmonic spectra in aligned molecules [14, 15].

The HHG process can be understood in the formalism of the three-step recollision model [16, 17]. In step 1, an electron is tunnel-ionized from a given bound electronic state, in step 2, it is first accelerated away then back towards its parent ion to, finally, in step 3, photorecombine back to its ground state via a dipolar transition. When multiple electronic states contribute to HHG, the coherent sum of their high-harmonic emission leads to an interference controllable by molecular alignment and the driving laser field parameters, such as the peak intensity [14, 18] and wavelength [19]. The first step of HHG is the strong-field ionization of the molecule. This step depends on the orientation of the molecule relative to the polarization direction of the laser. Depending on the orientation, different orbitals might be active.

Strong-field ionization of atoms has been extensively modelled, based on the Ammosov-Delone-Krainov (ADK) model [20–22]. This atomic model has been developed further [23], and was generalized to molecules in a technique called molecular ADK, or MO-ADK [24, 25].

In this paper, we present the first simultaneous measurements of strong-field ionization (SFI) and high-harmonic yield as a function of the molecular alignment in aligned molecules: N_2 and CO_2. Keeping the alignment conditions unchanged, we systematically survey the effect of changing the driving field wavelength (800 nm and 1200 nm) and intensity ($I_{probe} = 0.8 - 2.3 \times 10^{14}$ W/cm^2).

We observe that, at 800 nm probe wavelength, HHG and SFI strongly depend on intensity for both N_2 and CO_2. In N_2, both ionization and HHG always peak when molecules are aligned parallel to the driving field ($\alpha = 0°$). When the intensity of the latter is increased, the angular modulation becomes slightly weaker for the harmonic yield and significantly less pronounced for the molecular frame ionization. We observe the onset of ionization saturation around $I_{probe} = 2.0 \times 10^{14}$ W/cm^2. While the maximum angular modulation of the high-harmonic signal always occurs in the cutoff spectral region at 800 nm, independently of the laser intensity, it rather always occurs around 40 eV at 1200 nm probe wavelength. These measurements of HHG in aligned N_2 at longer wavelength (than 800 nm) provide evidence for dynamical effects that take place, along the lines of multiple orbitals ionization-induced hole dynamics [26].

In CO_2, we follow the position of the spectral minimum at both 800 and 1200 nm and see intensity-dependent structures which were not reported earlier [14]. In addition, the simultaneous measurement of SFI allows us to observe the onset of a sharp molecular frame angular ionization profile peaking around 42° as the laser intensity is decreased. This trend qualitatively agrees with previous experimental results on SFI in CO_2 [27].

II. EXPERIMENTAL RESULTS AND DISCUSSION

A. Impulsive molecular alignment

A Ti:Sapphire multi-pass laser system (32 fs, 800 nm, 50 Hz, 12 mJ per pulse) was used to perform all measurements. The molecules were first impulsively aligned

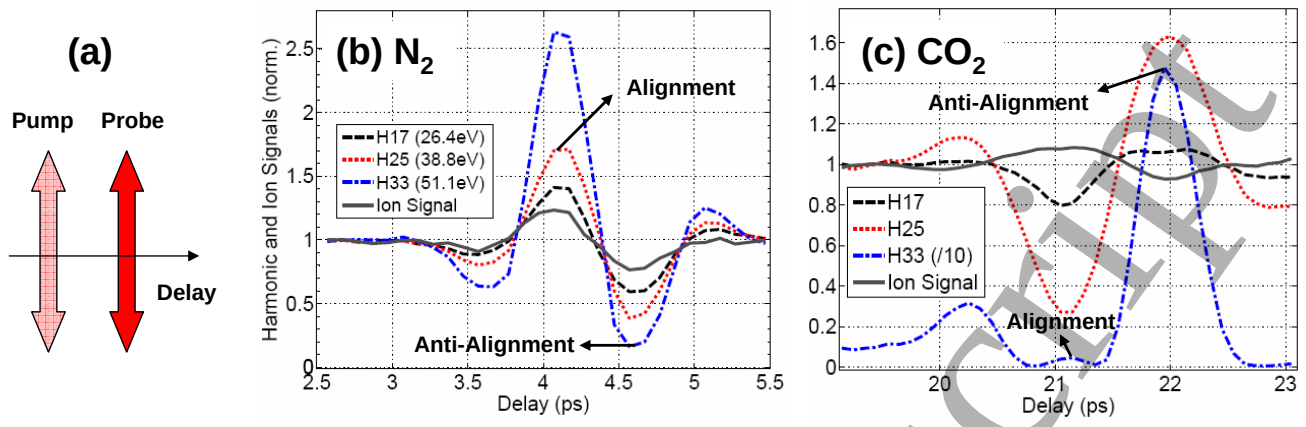

Figure 1. Rotational wavepackets are created via impulsive alignment with an 800 nm laser pulse. The molecules periodically rephase at revival times that depend on the molecule (8.4 ps for N_2 and 42.7 ps for CO_2). Here the molecules are probed around the half-revival times with an intense 800 nm laser pulse with an intensity of 1.5×10^{14} W/cm^2. (a) shows that parallel polarizations were used for the pump and probe pulses. The results for ionization yield and high-order harmonics are shown for (b) N_2 and (c) CO_2. At the time of maximum alignment (shown by arrows), the molecular internuclear axis distribution is prolate along the pump pulse polarization and has a 3D degree of alignment estimated to be $\langle \cos^2 \theta' \rangle = 0.60 \pm 0.05$ for our experimental conditions. At the time of anti-alignment, the molecular axes are mostly aligned perpendicular to the laser polarization.

[28, 29] using a stretched non-ionizing pump pulse (70 ± 5 fs, 800 nm, $I_{\text{align}} = 5 \times 10^{13}$ W/cm^2). After a delay time, the molecules were probed with a more intense laser pulse (800 nm: 32 ± 2 fs or 1200 nm: 40 ± 5 fs of variable intensity). The probe pulse served to ionize the molecules, and at the same time to create an XUV spectrum by high harmonic generation (HHG). In addition to the 800 nm pulses from the Ti:Sa laser system, 1200 nm pulses (~ 1 mJ) were generated by a high-energy optical parametric amplifier (HE-TOPAS) seeded by a fraction of the laser output (~ 8 mJ). The intensity was adjusted with neutral density filters in both pump and probe arms of the Mach-Zehnder interferometer. The polarization of the pump pulse was controlled by a half-wave plate.

The linearly polarized pump and probe beams were focused (f = 50 cm) into the supersonic gas jet emanating from a pulsed valve (Parker) that introduced the analyte molecule (N_2 or CO_2). The laser pulses were focused $\sim$2 mm before the gas target to select the HHG short trajectories [30], and $\sim$1 mm away from the pulsed valve orifice (250 μm diameter) in order to obtain cooler molecules. A negatively biased wire mesh located 10 cm from the nozzle orifice recorded the production of cations, which is a measure of the volume-integrated ionization probability. The linearity of this ion detector was verified [31]. The HHG spectra were recorded by an extreme ultraviolet (XUV) spectrometer composed of a concave XUV flatfield grating, a microchannel plate detector backed by a phosphor screen and a camera readout.

In Fig. 1, we present the time evolution of rotational wave packets as probed by high-harmonic and ionization yield measurements in (b) N_2 and (c) CO_2 molecules around their respective half-revival times. The high harmonic yields are spectrally integrated over a single harmonic order. The polarization directions of the aligning ($I_{\text{align}} = 5 \times 10^{13}$ W/cm^2) and probing ($I_{\text{probe}} = 1.5 \times 10^{14}$ W/cm^2) pulses are parallel. In N_2 (CO_2), the maximum degree of alignment is achieved at $\sim$4.12 ps ($\sim$21.15 ps) pump-probe delay corresponding to half-revivals [6, 7, 32]. When alignment occurs, the molecular internuclear axis distribution is prolate (cigar shaped) along the pump pulse polarization. Shortly following is anti-alignment (see Fig. 1(b) and (c)) where the alignment distribution becomes oblate [32] (pancake shaped). At maximum alignment, for both N_2 and CO_2, our experimental conditions ($P_{back} = 2$ atm., $T_{rot} = 30$-40 K, $I_{\text{align}} = 5 \times 10^{13}$ W/cm^2 and $\tau_{align} = 70 \pm 5$ fs) suggest a 3D degree of alignment of $\langle \cos^2 \theta' \rangle = 0.60 \pm 0.05$ based on calculations [33] and supported by supersonic gas expansion studies in similar conditions [34].

In N_2 (Fig. 1b), both the high-harmonic and ionization yields maximize when molecules are aligned parallel to the probing field (delay$\sim$4.12 ps). The ratio of signal aligned:anti-aligned in ionization is around 1.5:1 and increases monotonically with high-harmonic order, exceeding 10:1 for cutoff harmonics.

In CO_2 (Fig. 1c), in contrast to the case of N_2, the high-harmonic yield generally anti-correlates with ionization. This anti-correlation, reported earlier in ref.[7], suggested evidence for two-center destructive quantum interference taking place at the recombination step in aligned CO_2 molecules [35]. However, the presence of a dynamical (laser-dependent) local maximum in high-harmonic yield at alignment in the cutoff region (see H33 in Fig. 1c) is due to the dynamical interplay of multiple orbitals [14, 19].

We now proceed to study the dependence of both ion-

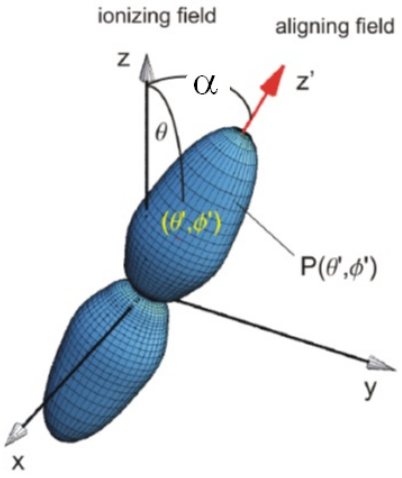

Figure 2. Definition of the molecular frame of reference. The distribution of molecular angles in the laboratory frame is given by $P(\theta', \phi')$. The angle of an individual molecule to the laboratory Z axis is θ.

ization and high-harmonic yields as a function of alignment angle α between the alignment and HHG probe polarization axes. For this, in aligned N_2 (CO_2), we set the pump-probe delay to ∼4.12 ps (∼21.15 ps) and rotate the polarization axis of the pump pulse with a half wave plate.

B. Strong field ionization in aligned molecules

The ionization signal measured in the laboratory frame (LF) $S(\alpha)$, is a convolution of the molecular frame (MF) ionization profile $I(\theta)$ with the prolate molecular internuclear axis distribution $P(\theta', \phi')$. Here θ is the angle between the laser field polarization and the molecule's internuclear axis. The geometry is shown in Fig. 2. In integral form,

$$S(\alpha) = \int_{\theta'=0}^{\theta'=\pi} \int_{\phi'=0}^{\phi'=2\pi} I(\theta(\theta', \phi', \alpha)) P(\theta', \phi') \sin\theta' \mathrm{d}\phi' \mathrm{d}\theta' \tag{1}$$

$\theta(\theta', \phi', \alpha)$ is defined by the LF to MF coordinate transformation [27],

$$\cos\theta = \cos\alpha\cos\theta' - \sin\alpha\sin\theta'\sin\phi' \tag{2}$$

The experimental ionization yield $S(\alpha)$ is recorded as a function of the angle α between the aligning pulse polarization and that of the probe pulse. We wish to determine the molecular-frame ionization probability $I(\theta)$, which is convolved with the alignment distribution $P(\theta', \phi')$ via eq. 1. We parameterize $I(\theta)$ using the first 4 even normalized Legendre polynomials $l_i(\theta)$: $I(\theta) = \left|\sum_{i=0}^{3} a_{2i} l_{2i}(\theta)\right|$. We parametrize the molecular axis distribution $P(\theta', \phi')$ following ref. [27], using $\langle\cos^2\theta\rangle = 0.55, 0.6, 0.65$ to cover the uncertainty in the degree of alignment. A least-squared optimization procedure is used to determine the molecular frame ionization probability $I(\theta)$.

Figure 3 shows the LF ionization of N_2 (scatter) using a 800 nm probe pulse at three peak intensities. The deconvoluted MF ionization probability distributions $I(\theta)$ of N_2 are shown in green using $\langle\cos^2\theta'\rangle = 0.55$ (dashed), 0.60 (solid) and 0.65 (dotted). With a 800 nm probe and $I_{probe} = 1.0\times10^{14}$ W/cm^2, the ∼3:1 ratio between parallel to perpendicular alignment is consistent with previous studies and reflects the σ_g symmetry of the highest occupied molecular orbital (HOMO) of N_2 [27, 36–38]. The small local maximum of ionization featured at $\theta = 90°$ is real as it was also reported elsewhere at lower intensity ($I_{probe} = 3.0\times10^{13}$ W/cm^2) via COLTRIMS measurements [39]. As the intensity of the ionizing pulse increases, the parallel:perpendicular ratio decreases and the angular profile becomes almost isotropic. This is likely due to saturation of the ionization probability, which smooths out the angular dependence of ionization.

Figure 4 shows the same measurements in CO_2. In both N_2 and CO_2, more sharply peaked features in the MF ionization profiles are found at the lowest intensity (1.0×10^{14} W/cm^2) while more isotropic responses that could indicate saturation of single ionization are found at the highest intensity (2.3×10^{14} W/cm^2) . The most striking difference between MF strong field ionization profiles in N_2 and CO_2 is the presence of a maximum peaked at 0° in N_2 and a local minimum at the same angle for CO_2. In Fig. 4(a), the ionization maximizes close to 42°. This can be understood intuitively by considering the orbital structure of N_2, N_2^+, CO_2 and CO_2^+ given in table I. While the ground state of N_2 and CO_2 share the same Σ_g^+ symmetry, ionization from the HOMO leads to $\tilde{X}^2\Sigma_g^+$ in N_2^+ and to $\tilde{X}^2\Pi_g$ in CO_2^+. A $\Sigma \rightarrow \Sigma + |\epsilon, k\rangle$ transition has typically larger dipole matrix elements along the internuclear axis (N_2), and $\Sigma \rightarrow \Pi + |\epsilon, k\rangle$ transitions (CO_2) have larger dipole matrix elements at some intermediate angle (≈42°) from the internuclear axis. Another way to state this is the Dyson orbital that is "ionized" is Σ_g for N_2 and Π_u for CO_2 [40, 41].

These results are consistent with those reported by Pavičić et al. [27]. For the case of CO_2, the molecular frame ionization probability $I(\theta)$ in Pavičić are considerably sharper than the present results in Fig. 4. There are several possible causes of this difference. Pavičić used the lowest possible laser intensity to ionize the CO_2 molecules, and we can see from Fig. 4 that the angular distribution becomes less well defined with higher intensities. Pavičić directly measured the distribution function $P(\theta', \phi')$ by Coulomb-exploding the molecules. Higher charge states showed a narrower angular distribution, and so it may be that the direct measurement actually under-estimated the degree of alignment. The fitting procedure then forced the molecular-frame ionization probability $I(\theta)$ to be narrower to match the laboratory-frame measurement.

To investigate the dependence of the molecular frame

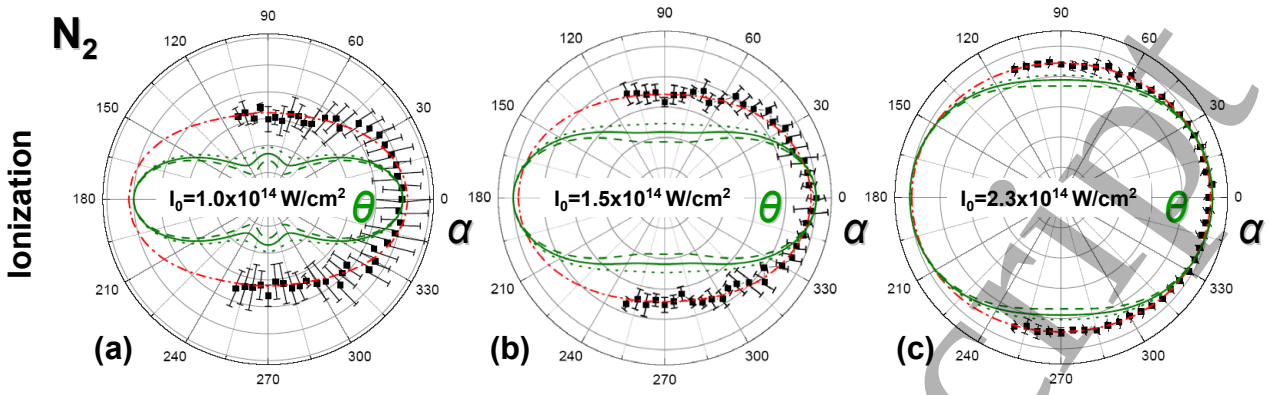

Figure 3. N_2 ionization signal vs alignment angle α with $\lambda = 800$ nm for different intensities of the driving field. $I_{probe} = 1.0$ (a), 1.5 (b) and 2.3 (c) $\times$ 10^{14} W/cm^2. From the laboratory frame ionization signal (scatter) and its Legendre polynomial fit (red dash-dotted line), we retrieved the MF ionization profile $I(\theta)$ using the degree of alignment $\langle cos^2\theta' \rangle = 0.55$ (dash), 0.60 (solid) and 0.65 (dotted).

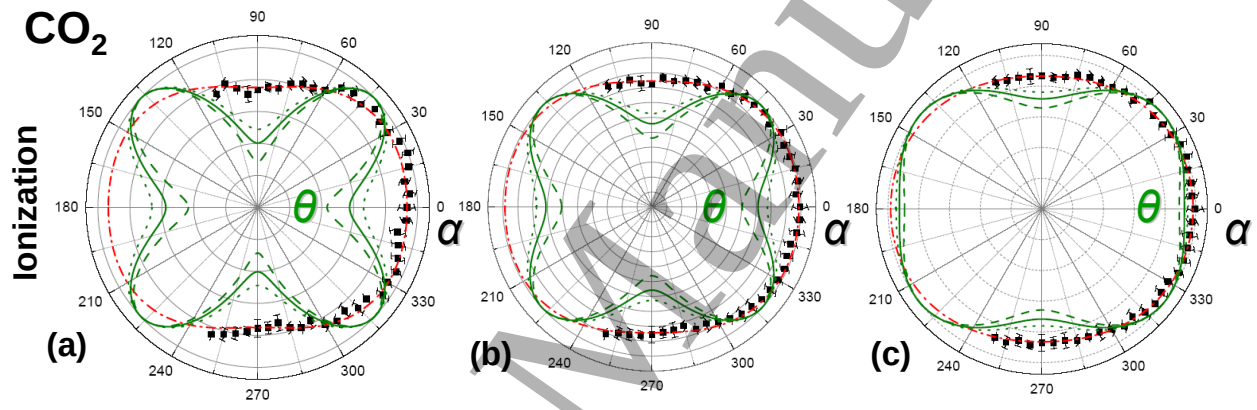

Figure 4. CO_2 ionization signal vs alignment angle α with $\lambda = 800$ nm for different intensities of the driving field. $I_{probe} = 1.0$ (a), 1.5 (b) and 2.3 (c) $\times$ 10^{14} W/cm^2. As in Fig. 3, we retrieved the MF ionization profile $I(\theta)$ using the degree of alignment $\langle cos^2\theta' \rangle = 0.55$ (dash), 0.60 (solid) and 0.65 (dotted) from the laboratory frame ion signal (scatter) and its Legendre polynomial fit (red dash-dotted line).

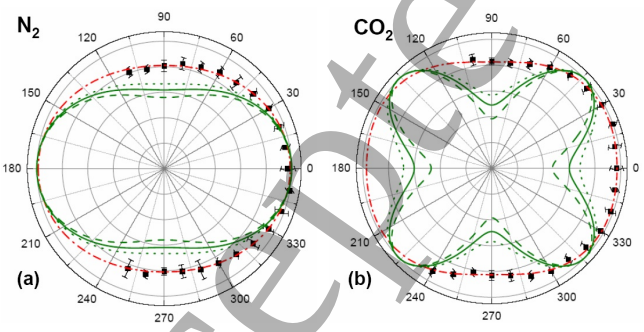

Figure 5. Strong field ionization vs alignment angle with $\lambda = 1200$ nm probe and intensity 1.1×10^{14} W/cm^2 (a) N_2 (b) CO_2. Legend is the same as in Figs. 3-4.

ionization $I(\theta)$ on the wavelength of the ionizing laser, the OPA output at 1200 nm was used instead of 800 nm. Figure 5 shows the measurements done with a probe wavelength of 1200 nm and intensity 1.1×10^{14} W/cm^2. The MF ionization profiles do not strongly depend on wavelength as profiles taken at 1200 nm (Fig. 5) are similar to those taken at 800 nm (Figs. 3 and 4). A clear comparison is difficult to make, as the laser intensities are difficult to determine exactly for the different wavelengths. The similarity between ionization at different wavelengths suggests that intermediate resonances in the multiphoton ladder leading to ionization do not play a major role in these molecules [42].

C. High harmonic emission from aligned molecules

The same experimental setup in the previous section, that measured the molecular-frame dependence of ionization yield, was used to record the molecular-frame dependence of high harmonic generation. As before, the polarization direction of the pump pulse that aligned the

Table I. Symmetry and energy of selected states of neutral and singly ionized N_2 and CO_2.

Species	State	configuration	ϵ (eV)
N_2	$X^1\Sigma_g^+$	$(1\sigma_g)^2(1\sigma_u)^2(2\sigma_g)^2(2\sigma_u)^2(1\pi_u)^4(3\sigma_g)^2$	0
N_2^+	$\tilde{X}^2\Sigma_g^+$	$[X^1\Sigma_g^+](3\sigma_g)^{-1}$	15.58
	$\tilde{A}^2\Pi_u$	$[X^1\Sigma_g^+](1\pi_u)^{-1}$	16.72
	$\tilde{B}^2\Sigma_u^+$	$[X^1\Sigma_g^+](2\sigma_u)^{-1}$	18.74
CO_2	$X^1\Sigma_g^+$	$(1\sigma_g)^2(1\sigma_u)^2(2\sigma_g)^2(3\sigma_g)^2(2\sigma_u)^2(4\sigma_g)^2$ $(3\sigma_u)^2(1\pi_u)^4(1\pi_g)^4$	0
CO_2^+	$\tilde{X}^2\Pi_g$	$[X^1\Sigma_g^+](1\pi_g)^{-1}$	13.78
	$\tilde{A}^2\Pi_u$	$[X^1\Sigma_g^+](1\pi_u)^{-1}$	17.31
	$\tilde{B}^2\Sigma_u^+$	$[X^1\Sigma_g^+](3\sigma_u)^{-1}$	18.07
	$\tilde{C}^2\Sigma_g^+$	$[X^1\Sigma_g^+](4\sigma_g)^{-1}$	19.39

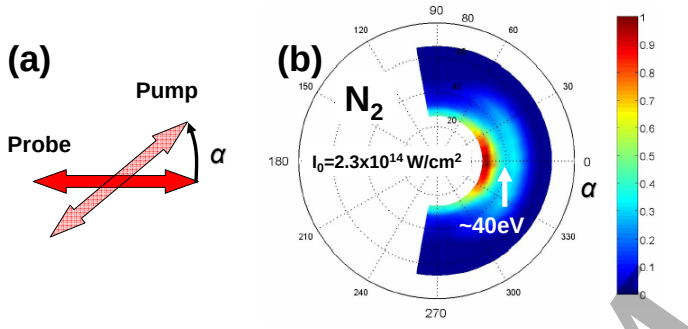

Figure 6. High-harmonic yield in aligned N_2 at $\lambda = 800$ nm as a function of alignment angle α. (a) shows the polarization arrangement between pump and probe pulses. (b) Experimental intensity of HHG from aligned N_2 molecules for a probe laser wavelength of 800 nm. $I_{probe} = 2.3 \times 10^{14}$ W/cm^2. $\alpha = 0$ means that the molecular axis is parallel to the polarization of the pulse the generates the high-harmonic emission. The radial axis goes from 0 to 80 eV. The color scale is linear with intensity.

molecules in space was rotated by an angle α; the probe pulse that generated the high-harmonic emission was always horizontal, so that the efficiency of the XUV spectrometer was the same. The polarization arrangement is shown in Fig. 6(a). The measurement covers the angular range α = -100 to 100° in steps of 5°, where each angular step is averaged over 1000 laser shots, and covers the spectral range of high-harmonic orders H=17-41. The HHG yields are plotted in polar coordinates, with the radial part corresponding to HHG photon energies from 0 to 80 eV. The emission occurs in discrete harmonics orders, but the color plots interpolate between them. The polar angle is α, with $\alpha = 0$ (horizontal) meaning that the molecular axis is parallel to the probe polarization axis that generated the HHG. The left and right halves of the polar plot are mirror images since there is no difference between the molecules at 0° and 180°.

In Fig. 6(b), the HHG yield as function of angle is shown for N_2 molecules probed with 800-nm laser pulses. The maximum emission occurs for $\alpha = 0$, and minimizes at $\alpha = 90°$. This pattern is consistent with emission being primarily due to the $3\sigma_g$ orbital of N_2. A prominent minimum at 40 eV is observed as reported earlier [1, 15, 19, 26, 43, 44]. This minimum essentially remains present at all alignment angles α and is independent of laser parameters [19], and is attributed to a shape resonance in the photoionization cross section of N_2. Another study reported a small spectral shift (∼5 eV) of this minimum [45].

There has been evidence reported of the appearance of a structure near the cutoff at $\alpha = 90°$ that is associated with HOMO-1 [18, 26, 45, 46], but is not apparent here. To explain this, it is suggested that, in addition to the HOMO (XX) and HOMO-1 (AA) channels, an electron can cross-recombine from HOMO to HOMO-1 (XA). RABBITT measurements [15] that led to the tomographic reconstruction of both HOMO and HOMO-1, suggest that the HOMO-1 channel is dominant at $\alpha = 90°$.

In Fig. 7, we present the high-harmonic yield of CO_2 as a function of alignment angle α at driving field wavelength $\lambda = 800$ nm and three intensities. HHG spectra taken at $\alpha = 0°$ are presented in Fig. 8 for three peak intensities. We observe a spectral minimum which moves from H25 (∼39 eV) to H29 (∼45 eV) on the intensity range covered. The intensity dependence of the position of this minimum was previously observed [7]. This feature is believed to be due to the interplay of multiple orbitals [14]. In aligned CO_2, at $\alpha = 0°$, the spectral minimum is attributed to destructive interference between the HOMO (X) and HOMO-2 (B) channels. Additional experimental observation of this dynamical minimum at $\alpha = 0°$ and longer driving field wavelength was reported ($\lambda = 1200$ nm [19] and $\lambda = 1300$ nm [47]) and supports the multiple orbitals interference model [14, 48–50].

Recent calculations [51] suggest that additional factors must be considered in the HHG from CO_2. They show that electron-electron correlations and dipole interchannel couplings in the cation must be included. These calculations support the experimental observation in Fig. 7 that the spectral minimum at $\alpha = 0°$ goes to higher energy as the laser intensity is increased. The predicted minimum [51] of 42 eV at 1.4×10^{14} W/cm^2 agrees exactly with our observation at 1.5×10^{14} W/cm^2 in Fig. 7(b) and Fig. 8.

At low driving intensity ($I_{probe} = 0.7 \times 10^{14}$ W/cm^2, see Fig. 7(a)), we observe that the high-harmonic yield of CO_2 peaks around $\alpha \approx 60 - 70°$ across the spectrum. This is consistent with EPOLYSCAT [52, 53] photorecombination transition dipole moments of the HOMO [54]. As the intensity increases, the angular profile peaks more around $\alpha = 90°$, see Fig. 7(b)-(c) which suggests the dominance of the HOMO-1 participation at that angle as expected from both its corresponding angular ionization profile and transition moments peaking in that direction [14]. Finally, at the maximum intensity ($I_{probe} = 2.3\times10^{14}$ W/cm^2, see Fig. 7(c)), the local maximum of signal above the spectral minimum (≥45 eV) in

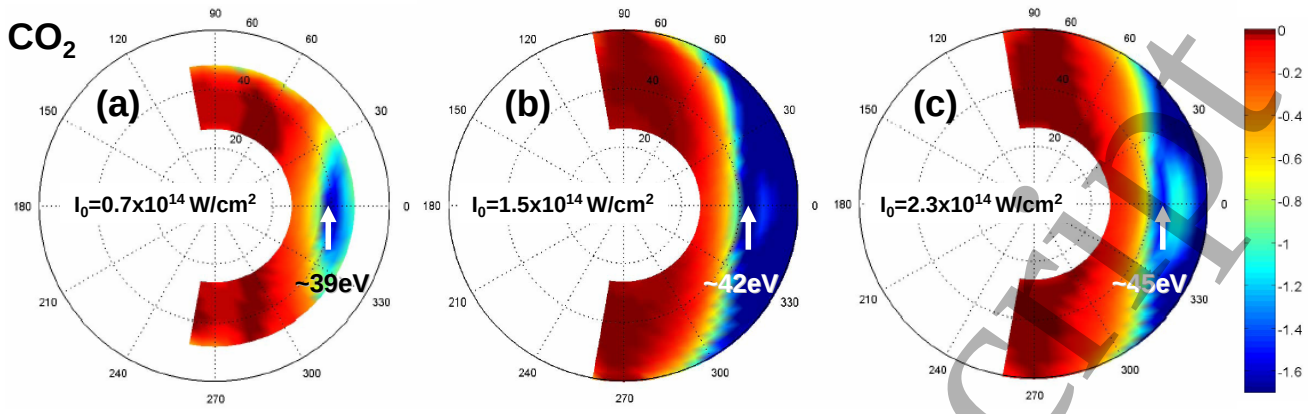

Figure 7. High-harmonic yield in aligned CO_2 with $\lambda = 800$ nm as a function of alignment angle. Experimental measurements at $I_{probe} = 0.7$ (a), 1.5 (b) and 2.3 (c) $\times\ 10^{14}$ W/cm^2. The radial scale is 0 to 60 eV. The intensity scale is logarithmic ($\log_{10}$). There is a characteristic minimum in the HHG spectrum for $\alpha = 0$ that shifts with laser intensity.

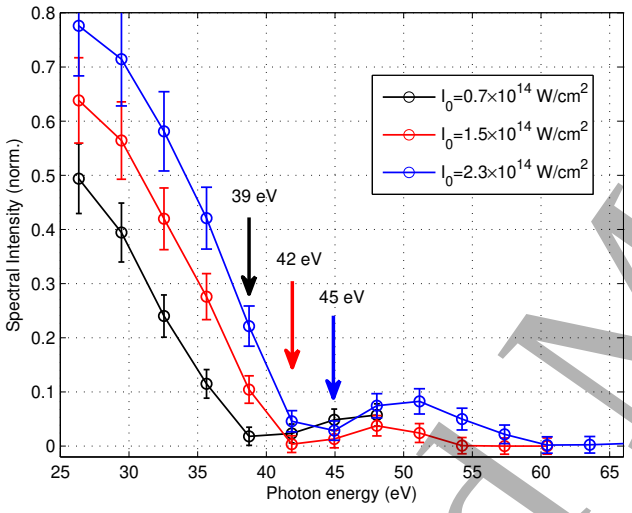

Figure 8. High-harmonic spectra in aligned CO_2 for $\alpha = 0°$, i.e. molecular axis is parallel to the probe laser polarization. The probe wavelength is $\lambda = 800$ nm. Experimental measurements at $I_{probe} = 0.7$ (black solid line), 1.5 (red dashed line) and 2.3 (blue dotted line) $\times\ 10^{14}$ W/cm^2. The minimum is seen to shift with increasing intensity to higher photon energy.

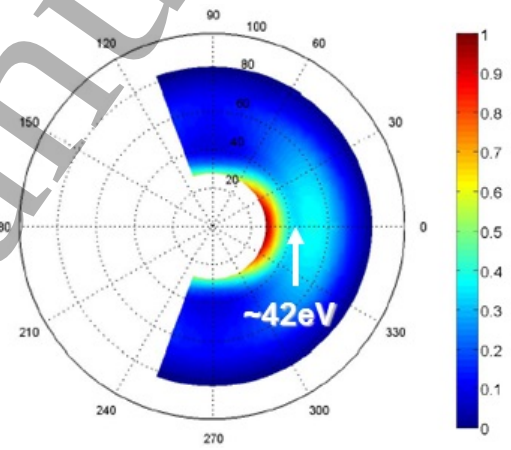

Figure 9. High-harmonic yield in aligned N_2 vs α with probe driving wavelength $\lambda = 1200$ nm. $I_{probe} = 1.1 \times 10^{14}$ W/cm^2. The color scale is linear in HHG emission intensity. Compared with measurements taken at 800 nm (Fig. 6), the HHG spectrum has changed little at this wavelength.

the vicinity of $\alpha = 0°$ has grown relatively to the overall yield, compared to $I_{probe} = 1.5 \times 10^{14}$ W/cm^2 (see Fig. 7 (b)), which roughly goes along with the increasing participation of HOMO-2. Therefore, we have shown that the angular high-harmonic yield profile depends strongly on intensity, giving insight into the participation of molecular orbitals.

HHG spectra of N_2 taken with 1200 nm probe pulses are shown in Fig. 9. As discussed in Ref. 19, the position of the HHG minimum in N_2 is fairly insensitive to laser parameters, as can be seen by direct comparison of Fig. 6(b) and of Fig. 9.

Figure 10 shows the HHG yield in CO_2 for a probe laser wavelength of 1200 nm. The minimum around $\alpha = 0$ moves significantly towards higher photon energy with increasing intensity in the range $I_{probe} = 1.2 \times 10^{14}$ W/cm^2 [19]. It has been reported to reverse direction at higher intensity [47]. We have observed that when increasing the intensity to $I_{probe} \geq 1.5 \times 10^{14}$ W/cm^2, the minimum remains around 58 eV (not shown) and we have not seen the direction to reverse.

III. CONCLUSIONS AND PERSPECTIVES

The behaviour of the HHG spectra for N_2 and CO_2 around $\alpha = 0$, i.e. when the laser polarization axis is parallel to the molecular axis, illustrates two contrasting mechanisms. The minimum in N_2 around 40 eV is largely independent of laser intensity and wavelength, and is an example of a *structural* minimum. The Cooper minimum

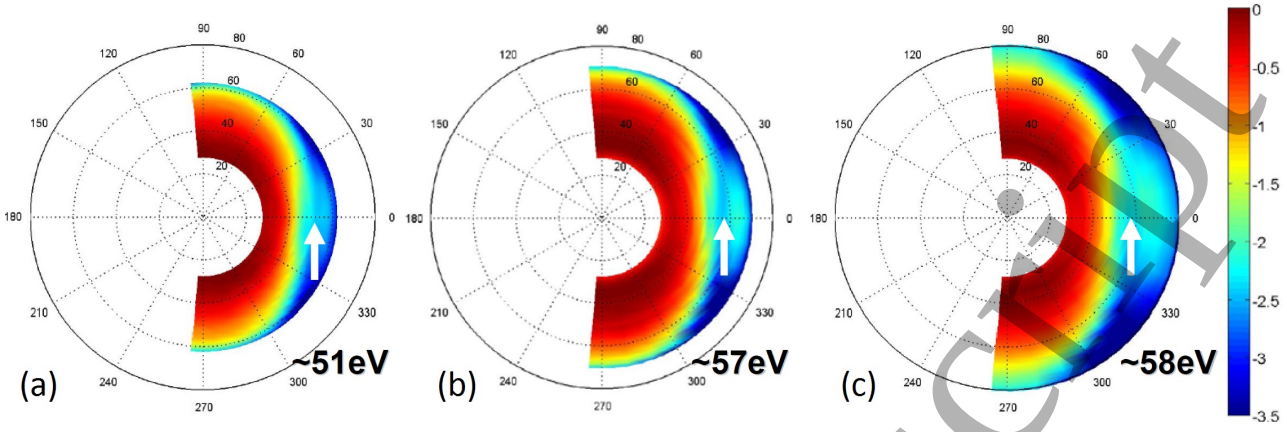

Figure 10. (a) High-harmonic yield in aligned CO_2 as a function of alignment angle for $\lambda = 1200$ nm for three probe intensities. The radial axis goes from 0 to 80 eV for all plots. The intensity scale is logarithmic ($\log_{10}$)

.

in argon is an example of a structural minimum, whereby the photoionization cross section minimizes due to a sign change in one of the partial wave components [55].

On the other hand, the on-axis HHG minimum seen in CO_2 is an example of a *dyamical* minimum, which is caused be the contribution of a deeper-bound orbital. In CO_2 at $\alpha = 0$, the contribution of the HOMO-1 orbital is minimized, allowing the HOMO-2 to become apparent. Because the HOMO-2 has a higher ionization potential compared with the HOMO, it contributes to a higher cutoff energy in the HHG spectrum, where the HOMO contribution is falling. It is the coherent interference between HHG contributions from these orbitals that leads to the minimum in the HHG spectrum near the cutoff energy. As the laser intensity increases, so too does the location of the interference minimum. By going to longer laser wavelengths, the *structural* minimum of CO_2 becomes apparent [56].

High harmonic generation has three steps: ionization, acceleration, and recombination. The simultaneous measurement of molecular-frame ionization probability and the HHG yield will permit the deconvolution of the HHG yield from the laboratory-frame measurement to the molecular frame [57], effectively removing the first step from the three-step model. This will improve the sensitivity of the measurement to the molecular-frame recombination matrix elements, and may provide more information on the molecular origins of HHG spectra.

ACKNOWLEDGMENTS

We gratefully acknowledge support from the Joint Centre for Extreme Photonics.

[1] J. Itatani, J. Levesque, D. Zeidler, H. Niikura, H. Pépin, J. C. Kieffer, P. B. Corkum, and D. M. Villeneuve, Nature (London) **432**, 867 (2004).

[2] S. Haessler, J. Caillat, W. Boutu, C. Giovanetti-Teixeira, T. Ruchon, T. Auguste, Z. Diveki, P. Breger, A. Maquet, B. Carré, et al., Nature Physics **6**, 200 (2010), ISSN 1745-2473.

[3] C. Vozzi, M. Negro, F. Calegari, G. Sansone, M. Nisoli, S. De Silvestri, and S. Stagira, Nature Physics **7**, 822 (2011).

[4] H. J. Wörner, J. B. Bertrand, D. V. Kartashov, P. B. Corkum, and D. M. Villeneuve, Nature (London) **466**, 604 (2010).

[5] C. Altucci, R. Velotta, and J. Marangos, Journal of Modern Optics **57**, 916 (2010).

[6] J. Itatani, D. Zeidler, J. Levesque, M. Spanner, D. M. Villeneuve, and P. B. Corkum, Phys. Rev. Lett. **94**, 123902 (2005).

[7] T. Kanai, S. Minemoto, and H. Sakai, Nature (London) **435**, 470 (2005).

[8] N. L. Wagner, A. Wüest, I. P. Christov, T. Popmintchev, X. Zhou, M. M. Murnane, and H. C. Kapteyn, Proceedings of the National Academy of Sciences **103**, 13279 (2006), http://www.pnas.org/content/103/36/13279.full.pdf+html, URL `http://www.pnas.org/content/103/36/13279.abstract`.

[9] W. Li, X. Zhou, R. Lock, S. Patchkovskii, A. Stolow, H. C. Kapteyn, and M. M. Murnane, Science **322**, 1207 (2008), URL `http://www.sciencemag.org/cgi/content/abstract/322/5905/1207`.

[10] S. Baker, J. S. Robinson, C. A. Haworth, H. Teng, R. A. Smith, C. C. Chirila, M. Lein, J. W. G. Tisch, and J. P. Marangos, Science **312**, 424 (2006).

[11] H. J. Wörner, J. B. Bertrand, P. B. Corkum, and D. M. Villeneuve, Phys. Rev. Lett. **105**, 103002 (2010).

[12] E. Goulielmakis, Z.-H. Loh, A. Wirth, R. Santra, N. Rohringer, V. S. Yakovlev, S. Zherebtsov, T. Pfeifer, A. M. Azzeer, M. F. Kling, et al., Nature **466**, 739 (2010).

[13] A. Fleischer, H. J. Wörner, L. Arissian, L. R. Liu, M. Meckel, A. Rippert, R. Dörner, D. M. Villeneuve, P. B. Corkum, and A. Staudte, Phys. Rev. Lett. **107**, 113003 (2011), URL `http://link.aps.org/doi/10.1103/PhysRevLett.107.113003`.

[14] O. Smirnova, Y. Mairesse, S. Patchkovskii, N. Dudovich, D. M. Villeneuve, P. B. Corkum, and M. Y. Ivanov, Nature (London) **460**, 972 (2009).

[15] S. Haessler, J. Caillat, W. Boutu, C. Giovanetti-Teixeira, T. Ruchon, T. Auguste, Z. Diveki, P. Breger, A. Maquet, B. Carré, et al., Nature Physics **6**, 200 (2010).

[16] P. B. Corkum, Phys. Rev. Lett. **71**, 1994 (1993).

[17] P. B. Corkum and F. Krausz, Nature Physics **3**, 381 (2007).

[18] B. K. McFarland, J. P. Farrell, P. H. Bucksbaum, and M. Gühr, Science **322**, 1232 (2008).

[19] H. J. Wörner, J. B. Bertrand, P. Hockett, P. B. Corkum, and D. M. Villeneuve, Phys. Rev. Lett. **104**, 233904 (2010).

[20] A. M. Perelemov, V. S. Popov, and M. V. Terent'ev, Sov. Phys. JETP **23**, 924 (1966).

[21] M. V. Ammosov, N. B. Delone, and V. P. Krainov, JETP **64**, 1191 (1986).

[22] N. B. Delone and V. P. Krainov, Uspekhi Fizicheskikh Nauk **41**, 469 (1998).

[23] G. L. Yudin and M. Y. Ivanov, Phys. Rev. A **64**, 013409 (2001).

[24] X. M. Tong, Z. X. Zhao, and C. D. Lin, Phys. Rev. A **66**, 033402 (2002).

[25] T. Otobe, K. Yabana, and J.-I. Iwata, Phys. Rev. A **69**, 053404 (2004).

[26] Y. Mairesse, J. Higuet, N. Dudovich, D. Shafir, B. Fabre, E. Mével, E. Constant, S. Patchkovskii, Z. Walters, M. Y. Ivanov, et al., Phy. Rev. Lett. **104**, 213601 (2010).

[27] D. Pavičić, K. F. Lee, D. M. Rayner, P. B. Corkum, and D. M. Villeneuve, Phys. Rev. Lett. **98**, 243001 (2007).

[28] F. Rosca-Pruna and M. J. J. Vrakking, Phys. Rev. Lett. **87**, 153902 (2001).

[29] H. Stapelfeldt and T. Seideman, Rev. Mod. Phys. **75**, 543 (2003).

[30] P. Salières, A. L'Huillier, and M. Lewenstein, Phys. Rev. Lett. **74**, 3776 (1995).

[31] A. D. Shiner, C. Trallero-Herrero, N. Kajumba, H.-C. Bandulet, D. Comtois, F. Légaré, M. Giguere, J.-C. Kieffer, P. B. Corkum, and D. M. Villeneuve, Phys. Rev. Lett. **103**, 073902 (2009).

[32] P. W. Dooley, I. V. Litvinyuk, K. F. Lee, D. M. Rayner, M. Spanner, D. M. Villeneuve, and P. B. Corkum, Phys. Rev. A **68**, 023406 (2003).

[33] Y. Mairesse, N. Dudovich, D. Zeidler, M. Spanner, D. M. Villeneuve, and P. B. Corkum, J. Phys. B: At. Mol. Opt. Phys. **43**, 065401 (2010).

[34] K. Yoshii, G. Miyaji, and K. Miyazaki, Optics Letters **34**, 1651 (2009).

[35] M. Lein, N. Hay, R. Velotta, J. Marangos, and P. Knight, Phys. Rev. Lett. **88**, 183903 (2002).

[36] S. Petretti, Y. V. Vanne, A. Saenz, A. Castro, and P. Decleva, Phys. Rev. Lett. **104**, 223001 (2010).

[37] S. Petretti, Á. Magaña, A. Saenz, and P. Decleva, Physical Review A **94**, 053411 (2016).

[38] P. Hoerner, M. K. Lee, and H. B. Schlegel, The Journal of Chemical Physics **151**, 054102 (2019), ISSN 0021-9606.

[39] I. Thomann, R. Lock, V. Sharma, E. Gagnon, S. T. Pratt, H. C. Kapteyn, M. M. Murnane, and W. Li, J. Phys. Chem. A **112**, 9382 (2008).

[40] S. Patchkovskii, Z. Zhao, T. Brabec, and D. M. Villeneuve, Phys. Rev. Lett. **97**, 123003 (2006).

[41] S. Patchkovskii, Z. Zhao, T. Brabec, and D. M. Villeneuve, J. Chem. Phys. **126** (2007).

[42] M. Spanner and S. Patchkovskii, Chemical Physics **414**, 10 (2013), ISSN 0301-0104.

[43] Y. Mairesse, J. Levesque, N. Dudovich, P. B. Corkum, and D. M. Villeneuve, J. Modern Optics **55**, 2591 (2008), ISSN 0950-0340.

[44] S. B. Schoun, A. Camper, P. Salières, R. R. Lucchese, P. Agostini, and L. F. DiMauro, Physical Review Letters **118**, 033201 (2017).

[45] J. Farrell, B. McFarland, M. Gühr, and P. Bucksbaum, Chem. Phys. **366**, 15 (2009).

[46] J. Troß, X. Ren, V. Makhija, S. Mondal, V. Kumarappan, and C. A. Trallero-Herrero, Physical Review A **95**, 033419 (2017).

[47] R. Torres, T. Siegel, L. Brugnera, I. Procino, J. G. Underwood, C. Altucci, R. Velotta, E. Springate, C. Froud, I. C. E. Turcu, et al., Phys. Rev. A **81**, 051802(R) (2010).

[48] Y. Mairesse, J. Higuet, N. Dudovich, D. Shafir, B. Fabre, E. Mével, E. Constant, S. Patchkovskii, Z. Walters, M. Y. Ivanov, et al., Physical Review Letters **104**, 213601 (2010).

[49] A.-T. Le, R. R. Lucchese, M. T. Lee, and C. D. Lin, Phys. Rev. Lett. **102**, 203001 (2009).

[50] J. B. Bertrand, H. J. Wörner, P. Salières, D. M. Villeneuve, and P. B. Corkum, Nature Physics **9**, 174 (2013).

[51] M. Ruberti, P. Decleva, and V. Averbukh, Physical Chemistry Chemical Physics **20**, 8311 (2018).

[52] F. A. Gianturco, R. R. Lucchese, and N. Sanna, J. Chem. Phys. **100**, 6464 (1994).

[53] A. P. P. Natalense and R. R. Lucchese, J. Chem. Phys. **111**, 5344 (1999).

[54] A.-T. Le, R. R. Lucchese, S. Tonzani, T. Morishita, and C. D. Lin, Phys. Rev. A **80**, 013401 (2009).

[55] H. J. Wörner, H. Niikura, J. B. Bertrand, P. B. Corkum, and D. M. Villeneuve, Phys. Rev. Lett. **102**, 103901 (2009).

[56] C. Vozzi, M. Negro, F. Calegari, G. Sansone, M. Nisoli, S. D. Silvestri, and S. Stagira, Nature Physics **7**, 822 (2011).

[57] J. B. Bertrand, H. J. Wörner, P. Hockett, D. M. Villeneuve, and P. B. Corkum, Physical Review Letters **109**, 143001 (2012).